



Observation of seasonal asymmetry in the range spread F occurrence at different longitudes during low and moderate solar activity

Abimbola O. Afolayan¹, Mandeep Jit Singh^{1,2}, Mardina Abdullah^{1,2}, Suhaila M. Buhari^{2,3}, Tatsuhiro Yokoyama⁴, and Pornchai Supnithi⁵

¹Center of Advanced Electronic and Communication Engineering, Universiti Kebangsaan Malaysia, 43600 Bangi, Selangor, Malaysia

²Space Science Centre (ANGKASA), Institute of Climate Change, Universiti Kebangsaan Malaysia, 43600 Bangi, Selangor, Malaysia

³Geomatic Innovation Research Group, Faculty of Science, Universiti Teknologi Malaysia, 81310 Johor Bahru, Johor, Malaysia

⁴Research Institute for Sustainable Humanosphere, Kyoto University, Uji, Japan

⁵Faculty of Engineering, King Mongkut's Institute of Technology Ladkrabang, Bangkok, Thailand

Correspondence: Mandeep Jit Singh (mandeep@ukm.edu.my)

Received: 19 February 2019 – Discussion started: 27 February 2019

Revised: 10 July 2019 – Accepted: 10 July 2019 – Published: 21 August 2019

Abstract. A comparative study of the equatorial spread F occurrence was conducted at different longitudes during 2010 and 2013 representing the low (LSA) and moderate (MSA) solar activity periods respectively. The ionogram data were recorded at low-latitude stations including Jicamarca (JIC; 75.76° W, 8.17° S), Fortaleza (FZA; 38.52° W, 3.73° S), Ilorin (ILR; 7.55° E, 9.93° N), Chumphon (CPN; 88.46° E, 11° N) and Kwajalein (KWA; 167.73° E, 8.72° N). The range type spread F (RSF) occurrence was manually recorded at an hourly interval between 18:00 and 06:00 LT, and a monthly average of the RSF occurrence was estimated for each season. The longitudinal distribution of the RSF occurrence features included the observed difference in the onset time, the duration and the seasonal occurrence peak. The seasonal asymmetry in the RSF occurrence distribution was analysed in relation to the zonal drift reversal's effect on the plasma irregularity initiation. We believe that the inconsistent equinoctial asymmetry pattern in the RSF occurrence is modulated by the seasonal/longitudinal variation of the zonal drift reversal delay during both solar epochs. Likewise, the seeding effect and the background ionospheric condition were also considered as major factors influencing the frequency of irregularity generation in these regions.

1 Introduction

The equatorial spread F (ESF) is a nighttime phenomenon that describes the observed ionospheric F layer electron density irregularity within the equatorial or low-latitude regions and is usually depicted as the wide spread of the echo trace on the ionogram measurement (Booker and Wells, 1938; Bowman, 1990). This echo spread along the frequency band or height range is due to the scattered signal reflection from the multiple paths caused by the irregular ionospheric plasma density profile. The scale size of these plasma irregularities ranges between a few centimetres and hundreds of kilometres (Basu et al., 1978; De Paula et al., 2010). The ESF is usually initiated after the local sunset due to the rapid rise of the F layer, and this generates a steep bottom-side plasma density gradient as a result of the abrupt reduction of the E region ionization level. The Rayleigh–Taylor (R–T) instability excited in the bottom-side is considered to be the mechanism responsible for the initiation and non-linear growth of the plasma depletion (Woodman and La Hoz, 1976). The vertical plasma drift near the local post-sunset driven by the pre-reversal enhancement (PRE) of the zonal electric field is recognized as the major factor controlling the ESF morphology across the different seasons and longitudes (Abdu, 2001;

Dabas et al., 2003; Lee et al., 2005). The PRE rapidly elevates the ionosphere into a higher-altitude region, where the collision frequency is lower and more conducive for further plasma depletion growth by the R–T instability mechanism (Fejer et al., 1999; Woodman and La Hoz, 1976). However, recent studies (Candido et al., 2011; Narayanan et al., 2014; Stoneback et al., 2011) have also analysed the probable role of several other parameters involved in the plasma irregularity initiation over the period characterized by weak background ionospheric condition. The observation of a high ESF occurrence rate during the LSA has been attributed to the modulation of the post-sunset electrodynamic by the gravity wave (GW)-induced perturbation electric field (Abdu et al., 2009; Aveiro et al., 2009), whereas neutral wind intensity and direction is a dominant factor in the observed post-midnight ESF occurrence pattern (Dao et al., 2017; Sastri et al., 1994).

The plasma irregularity occurrence around the equatorial/low-latitude regions often distorts the L-band signal, causing poor performance of communication or navigation systems such as the global positioning system (GPS) (Aarons et al., 1997; Jiao and Morton, 2015). Therefore, it is important to understand the role of the different precursory factors influencing the spread F morphology under varying ionospheric conditions. This complex phenomenon has been explored widely by past studies (Su et al., 2009; Tsunoda, 2010a; Vichare and Richmond, 2005), and there are presently deliberate efforts to improve the prediction accuracy of the spread F occurrence distribution pattern across the different regions.

The complex interaction between the E and F region dynamo system in the presence of conductivities and the magnetic field are responsible for the different electrodynamic phenomenon in the low-latitude region (Haldoupis et al., 2003; Miller, 1997). During the daytime, the F region divergent current causes an accumulation of the downward polarization electric field on the bottom-side of the region. Conversely, the E region polarized electric field concurrently drives a closure current mapped along the magnetic field line into the F region that diminishes the F region vertical current (Abdu et al., 1981; Eccles et al., 2015; Heelis, 2004). The field-line-integrated Pedersen conductivity shorts out the F region dynamo electric field and significantly reduces the zonal plasma drift due to the high E region conductance during the daytime. However, the decay and the consequent reduction of the E region conductance during nighttime causes a significant increase in the field-aligned Pedersen conductivity ratio. This generates a large vertical current by the F region dynamo, and the resulting downward electric field drives the plasma in the direction of the neutral wind. Thus, the F layer dynamo electric field created by the divergence current dominates near the sunset period, and this induces the eastward plasma motion in the F region at an $E \times B$ velocity. The PRE vertical plasma drift is associated with the enhanced eastward electric field caused by the significant decay of the E region conductivity. This combined with the rapid

chemical recombination rate of the E layer around the sunset period results in the increased steepness of the bottom-side plasma density gradient. Hence, the large vertical drift enhances the plasma instability triggered by the seed perturbation and subsequently the R–T instability growth rate. In contrast, a prolonged eastward equatorial electrojet (EEJ) could cause a reduced field-aligned conductivity gradient due to the small vertical current driven by the post-sunset conjugate E region. Thus, the resulting zonal electric field accumulation at the F layer base can only generate a relatively small PRE vertical drift. This ionospheric electrodynamic effect also yields a zonal drift reversal delay, which has been shown to be a strong factor influencing the instability growth rate (Su et al., 2009). The seasonal/longitudinal distribution of the ESF occurrence rate is dependent on the declination angle of the magnetic field. The longitudinal gradient of the field-aligned Pedersen conductivity becomes steepest when the sunset terminator is well aligned with the local magnetic flux tube, thereby resulting in a simultaneous relative sunset time in the magnetic conjugate E regions that are coupled to the F region (Abdu et al., 1992; Maruyama and Matuura, 1984; Tsunoda, 1985; Tsunoda et al., 2015). Hence, the PRE of the eastward electric field is maximum at such a longitude and so is the elevation of the F layer altitude near sunset. The base of the F region is lifted to greater heights making it conducive for the plasma instability growth. Therefore, the longitudinal variation in the seasonal distribution of the ESF occurrence rate is associated with the variation of the solar terminator–magnetic field alignment (STBA) and their distinct local sunset time equatorial electric field system. Due to the near-zero sunset time lag between the conjugate E regions during the equinox period, there is usually a good alignment. Conversely, in several studies (Hoang et al., 2010; Su et al., 2008), the solstice months have been shown to have good (bad) alignments during the June solstice (December solstice) at longitudes of positive (negative) magnetic declination. The seasonal/longitudinal distribution of the equatorial plasma irregularity has been extensively reported to be strongly correlated with the seasonal variation of the STBA (Abdu et al., 1981; Li et al., 2008; Su et al., 2008). However, a recent study described the significant ESF occurrence during the solstice seasons in the West African and central Pacific regions as being inconsistent with the defined theory of the declination angle influence on the spread F longitudinal distribution (Tsunoda et al., 2015). These discrepancies are considered noteworthy for an improved understanding of the features of global plasma irregularity distribution as influenced by different background atmospheric conditions. This study is mainly focused on examining the salient features of the spread F local time distribution patterns at these longitude sectors during the equinox and solstice seasons of the low (2010: 80 sfu) and moderate (2013: 122.7 sfu) solar activity periods. Furthermore, the role of the zonal drift reversal time was investigated in relation to the observed asymmetry during the equinox and solstice seasons. While the asymme-

try pattern during the equinoxes is yet to be well defined and varies across the longitudes during both solar epochs, this analysis tended to understand the major phenomenon responsible for the equinoctial asymmetry of the ESF occurrence in each region. Thus, the probable competing role of the vertical plasma drift, virtual height and the seed perturbation were considered in the analysis of the observed spread F distribution at these longitude sectors.

2 Data and methods

The ESF events were recorded at equatorial stations situated at different longitudes (shown in Table 1): Jicamarca (JIC) station, Peru; Fortaleza (FZA) station, Brazil; Ilorin (ILR) station, Nigeria; Chumphon (CPN) station, Thailand; and Kwajalein (KWJ) station, the Republic of the Marshall Islands. Table 1 lists the geographic coordinates and the sunset time at each of the stations selected for the study of the spread F irregularity distribution. These are stations within the Southeast Asia low-latitude ionospheric network (SEALION) and the Global Ionospheric Radio Observatory (GIRO) network, as indicated in Fig. 1. The observation data were taken using the digital ionosonde (Digisonde model DPS-4) and analogue type FMCW (frequency modulated continuous wave) radar (Maruyama et al., 2008; Reinisch and Galkin, 2011). As the ESF events are very rare during the daytime, our investigation was limited to the time interval between 18:00 and 06:00 LT. The ionograms were examined at an hourly interval for the presence of range spread F (RSF) or strong range spread F (SSF). Subsequently, the monthly mean of the RSF occurrence percentage variation over the defined local time interval was then estimated using the following relation:

$$\begin{aligned} & \text{hourly occurrence \%} \\ &= \frac{(\text{number of ionograms in each hour with RSF})}{(\text{total number of ionograms in an hour for that month})} \\ & \times 100 \end{aligned} \quad (1)$$

Only the quiet days ($\Sigma\kappa p \leq 24$) were considered for each month representing the different seasons during the low ($F10.7A < 100$ sfu; $F10.7$ – solar flux index) and moderate ($F10.7A < 150$ sfu) solar activity period (Wang et al., 2017). The seasonal variation of the ESF events was analysed according to the available data at each of the ionosonde stations listed in Table 1. Thus, the data taken from the March, June, September and December months of 2010 (2013) represent the March equinox, June solstice, September equinox and December solstice of the LSA (MSA) respectively.

The recorded ionogram signatures are usually divided into frequency spread F (FSF), mixed spread F (MSF), range spread F (RSF) and strong range spread F (SSF) (Shi et al., 2011). However, this study considers only the RSF and SSF types during the observation of the plasma irregularity events recorded by the ionograms across these longitudes. The RSF

signature represents the instance of the ordinary F layer trace spreading mainly along the altitude as shown in Fig. 2, and the SSF, which is described as a type of RSF, has its ordinary trace extending significantly beyond the local foF2 (foF2 – critical frequency; Bowman, 1960, 1998). Hereafter, we will refer to the March, June, September and December seasons as the *M*-equinox, the *J*-solstice, the *S*-equinox and the *D*-solstice respectively.

The monthly average of the scaled virtual height was taken as a representation of the seasonal variation of the near-sunset vertical plasma drift recorded at each of the ionosonde stations. The seasonal variation of the virtual height taken during the low solar activity (LSA) and moderate solar activity (MSA) periods was then analysed in relation to the RSF occurrence distribution. Based on data availability across the considered stations (as shown in Fig. 3), the data taken during the year 2010 represent the LSA period, whereas the year 2013 represents the MSA period.

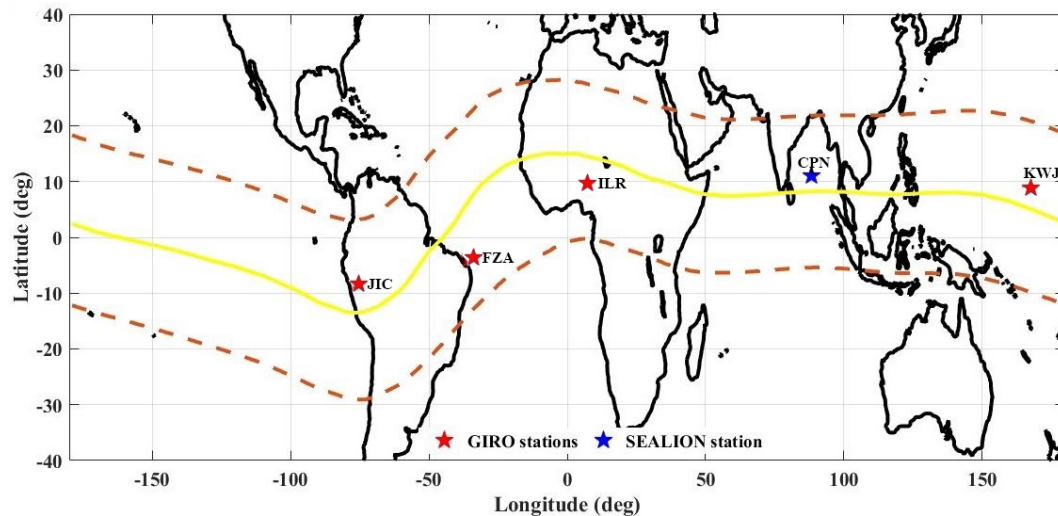
3 Results

Figures 4 and 5 present the hourly distribution of the RSF occurrence percentage across the different longitudes during the LSA period and the MSA period; this hourly distribution was averaged over each month based on the available data at these stations. The monthly mean RSF occurrence percentage was higher at all of the longitudes considered during the equinox months than during the solstice months of the LSA year. The RSF occurrence percentage and duration is highest at the ILR station for all the seasons, while the minimum monthly mean RSF occurrence percentage was recorded at the KWJ station. Generally, the average duration of the post-sunset plasma irregularity in Fig. 4, varies across these longitudinal sectors, while the starting time of the spread F during the equinox and *D*-solstice months varies mostly between 18:00 and 20:00 LT. The observed onset time variation of the RSF occurrence corresponds with the varying sunset time across the different longitudes as shown in Table 1, except for cases with significant delay. Figure 4 shows that the maximum RSF occurrence percentage was mostly observed before the midnight period (around 21:00 LT) during most seasons at each longitude. However, there are months that have a significantly larger RSF occurrence percentage near midnight than at 21:00 LT. This could be attributed to either the irregularity onset being delayed until the pre-midnight period as a result of the ionospheric condition or to multiple days with irregularities drifting from a distant location into the ionogram's field of view (Balan et al., 2018; Narayanan et al., 2014).

Another important observation was the large RSF occurrence percentage of $\sim 70\%$ at ILR but the relatively smaller occurrence rate of $\sim 30\%$ at KWJ during the *J*-solstice of the LSA year; the RSF occurrence percentage was below 10% in the other longitude regions. The large RSF occur-

Table 1. Description of the stations' geographic location and their local sunset time range.

Station	Longitude (°)	Latitude (°)	Dip latitude	Declination angle	Sunset time (LT)
Jicamarca (JIC)	-75.76	-8.17	3.75	-3.24	18:45–19:15
Fortaleza (FZA)	-38.52	-3.73	-6.89	-20.11	18:30–18:45
Ilorin (ILR)	4.5	8.53	-4.27	-1.69	18:00–19:00
Chumphon (CPN)	99.37	11	3.76	-1.46	19:30–20:15
Kwajalein (KWJ)	167.73	8.72	3.62	7.62	19:30–20:15

**Figure 1.** The geographic location of the ionosonde stations and their corresponding observatory network shown using the red (GIRO) and blue (SEALION) markers (yellow line and dashed brown line represent the Equator and $\pm 15^\circ$ latitudes, respectively) and .

rence percentage recorded at the ILR station was contrary to the expected longitudinal distribution based on the defined low and high ESF longitude range during the *J*-solstice (Su et al., 2007). Likewise, the other relevant observations across the different longitudes during the *J*-solstice, such as the significantly delayed irregularity onset at KWJ, will be further discussed in a later section.

Figure 5 shows that there was an increase of over 30% in the RSF occurrence percentage across all of the stations during the *M*-equinox of the MSA period. The spread *F*-equinox asymmetry was very visible in all of the regions except at the FZA station, where the hourly peak of the RSF occurrence percentage was approximately equal during both equinox seasons. Unlike the equinoctial asymmetry during the LSA which showed an inconsistent longitudinal variation, the *M*-equinox has a significantly larger RSF occurrence percentage at the CPN, JIC and KWJ stations during the MSA. Conversely, Figs. 4 and 5 show a similar solstice asymmetry in the observed RSF occurrence percentage during both solar epochs. The RSF occurrence percentage during the *J*-solstice of the MSA period was $\sim 10\%$ or less at all of the stations except at KWJ station. There was a $\sim 30\%$ increase in the RSF occurrence percentage at the KWJ station during *J*-solstice, and the irregularity onset time was also

much earlier (immediately after the local sunset) than the LSA onset time. Su et al. (2009) have already established a relationship between the zonal drift reversal time and the velocity drift amplitude, instability growth rate and irregularity onset in the $150\text{--}170^\circ$ longitude range. Hence, the delayed onset and the relatively small RSF occurrence percentage in this region during the LSA will later be discussed further in relation to the zonal drift reversal effect and the weak background ionospheric condition in the region.

The negative declination angle region was described as the high ESF longitude during the *D*-solstice due to the strong magnetic flux tube–solar terminator alignment (Tsunoda, 1985). Furthermore, the large declination angle in the Brazilian region causes a relatively simultaneous local sunset in the conjugate E region, thereby driving a stronger eastward polarization electric field in the equatorial F region (Abdu et al., 1981; Tsunoda, 2010a). Correspondingly, the highest RSF occurrence percentage peak was recorded at the FZA station for both the LSA ($\sim 85\%$) and MSA ($\sim 100\%$) period. The pre-midnight RSF occurrence percentage peak recorded a $\sim 15\%$ increase at the FZA and CPN stations during the *D*-solstice, while there was no RSF occurrence at the KWJ station during the MSA period. The reduced RSF occurrence percentage at KWJ during *D*-solstice correlates

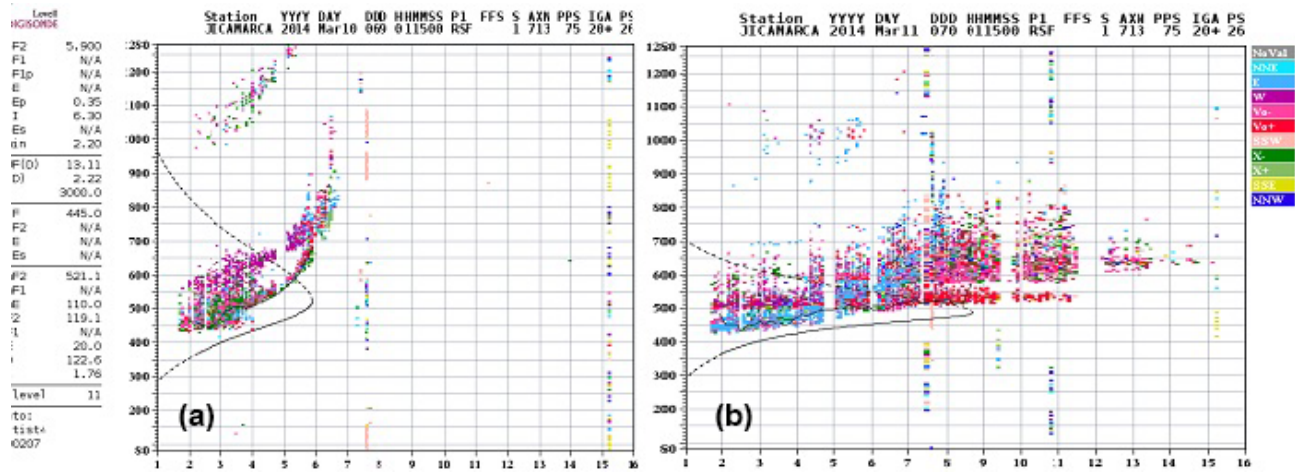


Figure 2. Sample of the RSF (a) and SSF (b) recorded using the DPS-4 digisonde at the Jicamarca station.

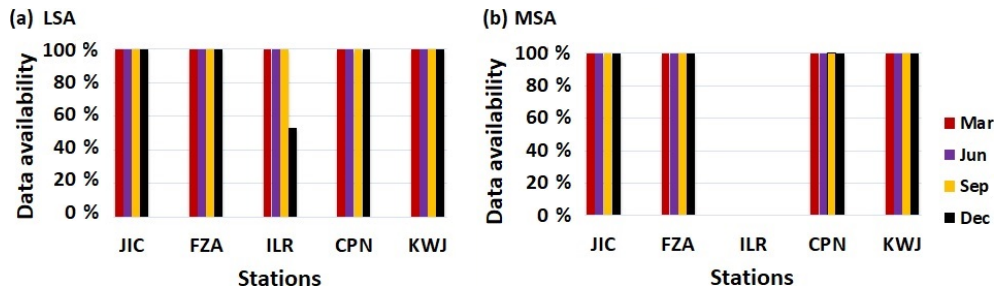


Figure 3. The ionogram data availability at the Jicamarca (JIC), Fortaleza (FZA), Ilorin (ILR), Chumphon (CPN) and Kwajalein (KWJ) stations during the (a) LSA and (b) MSA periods.

with the described anti-solar spread F occurrence pattern at the low ESF longitudes during the solstices (Su et al., 2007).

Figure 6a–d show a comparison between the RSF occurrence percentage during the MSA and LSA at each of the four stations with sufficient data. There was a significant difference between the spread F occurrence percentage during the LSA and MSA periods across all seasons at most of the stations except at JIC and FZA stations. The RSF occurrence percentage at both stations varied inversely with the solar flux index during *S*-equinox, whereas an approximately equal percentage was recorded during the *D*-solstice of both solar epochs. The observed negative solar flux dependence pattern at these longitudes during the *S*-equinox could be attributed to the growing effect of the density scale length on the irregularity growth during this season as the solar flux increases. Hence, the *S*-equinox and *D*-solstice seasons were described as having a more conducive ionospheric condition for the generation of RSF in this longitude region during LSA.

There was an absence of RSF occurrence at the JIC station during the *J*-solstice of the MSA. The inverse correlation between the solar flux intensity and the RSF occurrence has been observed at low ESF longitudes from 230 to 10° and

from 90 to 260° during the *J*-solstice and *D*-solstice respectively (Su et al., 2007) and was attributed to the neutral wind effect. This result was corroborated by the diverging neutral meridional wind pattern observed during the *J*-solstice at this longitude and the expected effect of the increased meridional wind on the irregularity growth suppression during the MSA. The peak RSF occurrence percentage at most of the longitudes during the LSA is usually around the midnight period, whereas the peak is closer to the local sunset time during MSA. However, thorough observation of the RSF occurrence features, as shown in Fig. 6a and b, indicated that the near-sunset peak and the rapid increase of the RSF occurrence percentage were more consistent for the seasons with an expectedly significant post-sunset rise (PSSR). The typical plasma irregularities formed around the sunset period are dominated by the PRE dynamics, while some other mechanisms may play a substantial role in the generation of the post-midnight ESF events (Dao et al., 2017; Otsuka, 2018).

Figure 7a and b show the local time variation of the monthly mean virtual height ($h'F$) during the LSA and MSA periods across the five longitude regions considered in this study. Likewise, the corresponding annual variation of the sunset time lag was also presented in Fig. 7c. This repre-

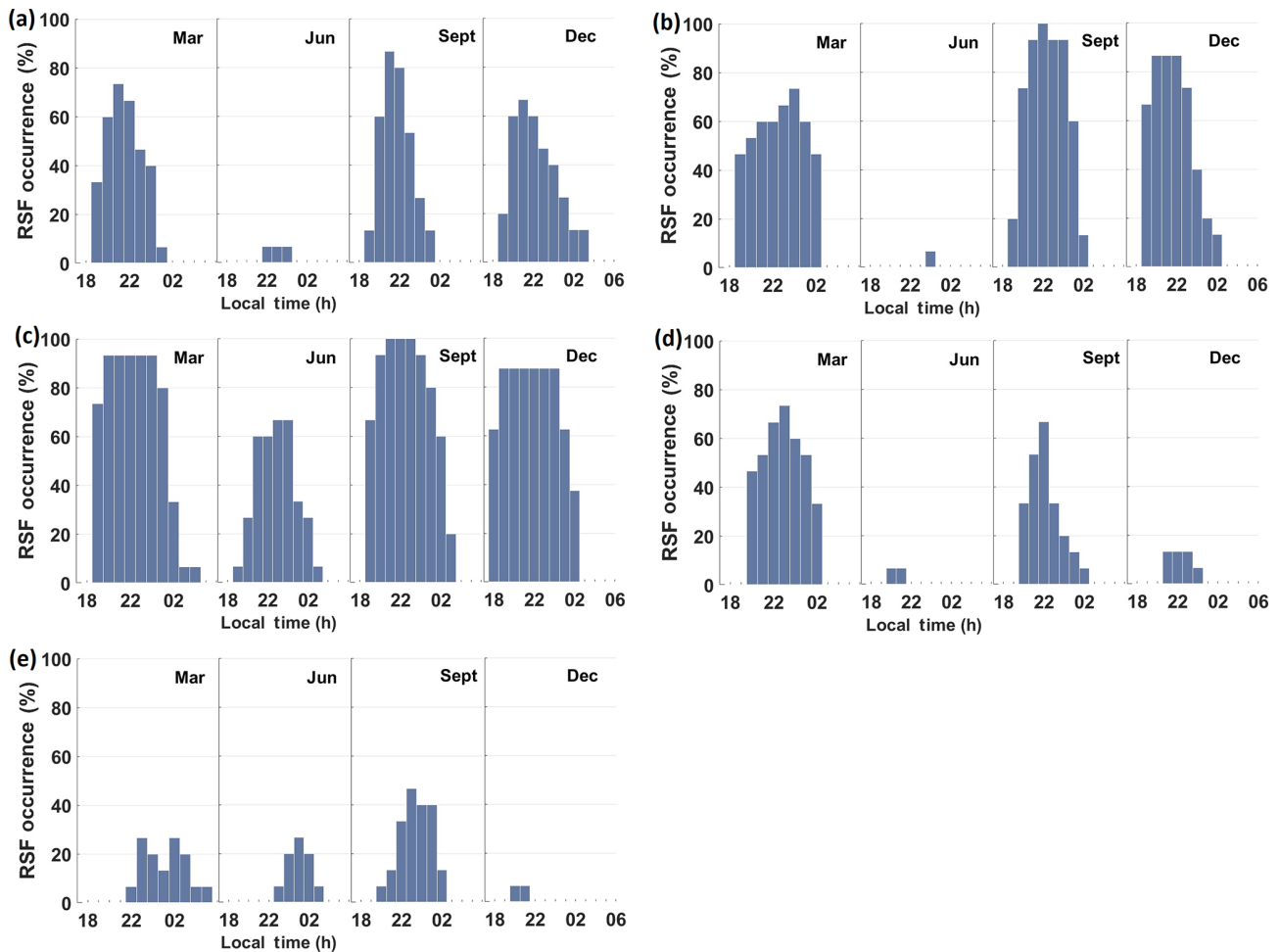


Figure 4. Occurrence rate of RSF during the LSA period at the (a) Jicamarca, (b) Fortaleza, (c) Ilorin, (d) Chumphon and (e) Kwajalein stations.

sents the difference between the local sunset times at the foot points of the conjugate E region that connects with the F layer base. The longitudinal variation pattern of the PSSR is consistent with the earlier numerical simulation by Vichare and Richmond (2005), which observed that the longitudinal PRE variation has its peak in a longitude region between 290 and 30° E. The observed PSSR of the $h'F$ (representing the pre-reversal enhancement, PRE, of the vertical plasma drift near the local sunset) is generally higher during the equinoctial and D -solstice months of MSA than the corresponding seasons of the LSA period. In the case of the J -solstice months, the near-sunset enhancement of the vertical plasma drift, as shown in Fig. 7a and b, was almost absent during both solar epochs. Although it is based on the comparison with the annual sunset time lag variation for each of the regions as shown in Fig. 7c, the PRE magnitude was expected to be larger at the KWJ station than in the other regions. However, the relatively large magnetic field strength in the Asian (CPN) and central Pacific (KWJ) regions (Su et al., 2009; Vichare and Richmond, 2005) causes the weak PRE mostly

observed in this regions during both solar epochs. Such zonal variation of factors including the eastward electric field, the field-aligned Pedersen conductivity and the magnetic field strength contributes to the resultant zonal variation of the vertical plasma amplitude (Abdu, 2016; Vichare and Richmond, 2005).

The sunset time lag was inconsistent with the observed solstice asymmetry in the PSSR in the low declination angle regions. The equatorial electrojet (EEJ) has been identified as a likely controlling factor in the seasonal variation of the near local sunset PSSR (Abdu et al., 1981). The effect of the post-sunset EEJ presence results from the strong dependence of the PSSR on the longitudinal gradient of the Pedersen conductivity. Hence, a seasonal modulation of the EEJ strength due to tidal winds from the lower atmosphere will contribute to the PRE. Apart from slow decay of the EEJ due to the prolonged sunset duration between the conjugate E regions, the seasonal ionospheric density variation could also influence the field-aligned current and the changes in the zonal drift reversal. Su et al. (2009) highlighted the influence of

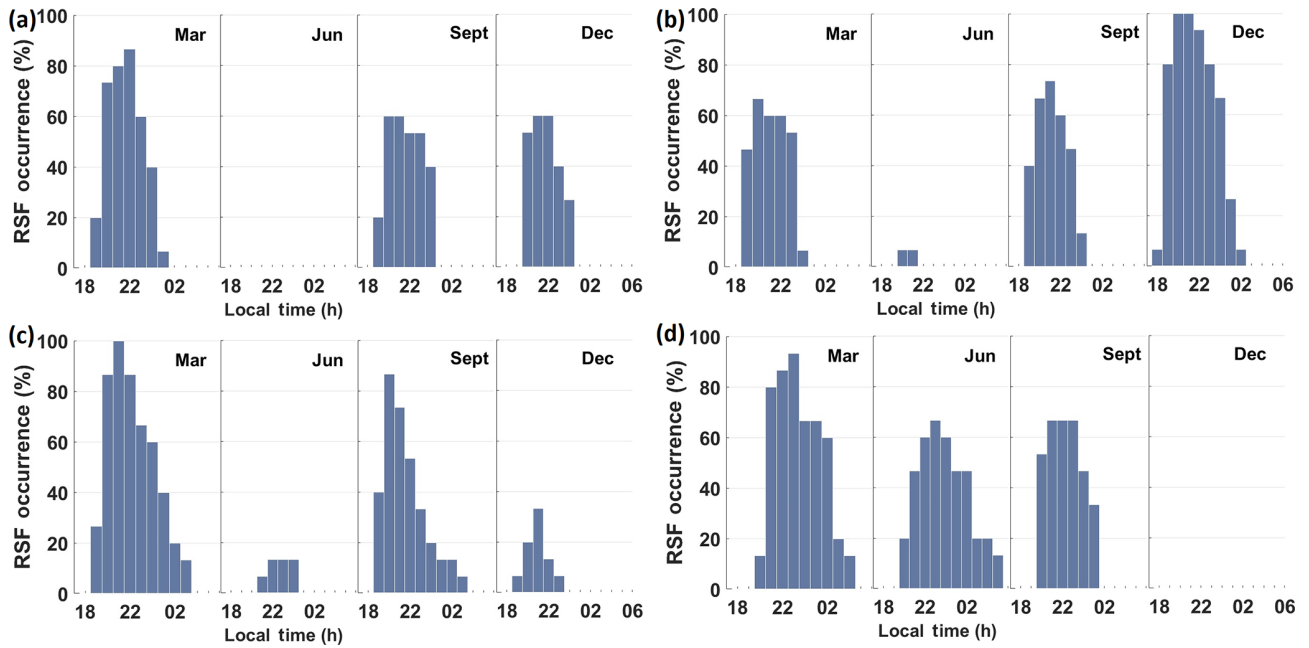


Figure 5. Occurrence rate of RSF during the MSA period at the (a) Jicamarca, (b) Fortaleza, (c) Chumphon and (d) Kwajalein stations.

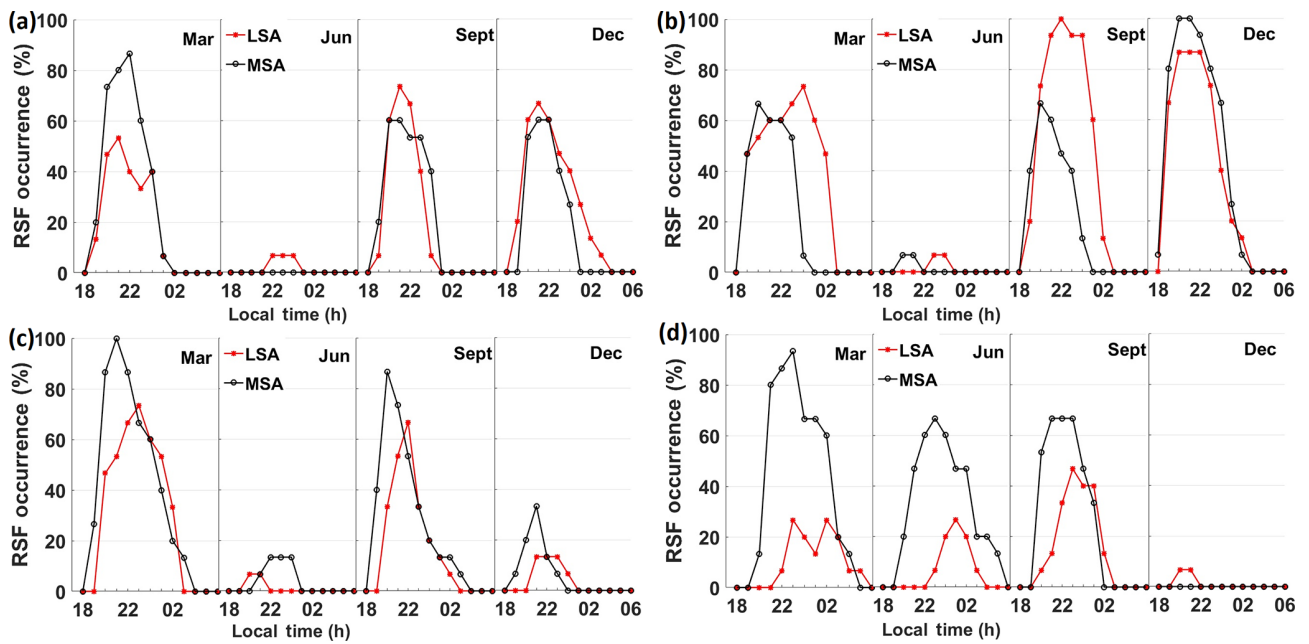


Figure 6. The percentage of ESF occurrences during the LSA and MSA periods for (a) Jicamarca, (b) Fortaleza, (c) Chumphon and (d) Kwajalein stations.

the prolonged eastward EEJ on the zonal drift reversal during J -solstice, which is expectedly accompanied by a weak vertical plasma drift in the F region. Conversely, an equinoctial asymmetry in the PSSR was also prominent during the MSA in all of the regions except at the KWJ station, where the weak E/B generally reduces the post-sunset PRE vertical drift. The asymmetry is mainly attributed to the increasing difference between the neutral density components at both equinoxes as the solar flux increases (Manju and Madhav Haridas, 2015).

4 Discussion

The observed longitudinal variation of the spread F occurrence during the different seasons of both solar epoch show a strong similarity to earlier studies (Klinngam et al., 2015; Pezzopane et al., 2013; Pietrella et al., 2017; Su et al., 2007; Tsunoda et al., 2015). These studies deployed different measurement techniques to establish a strong linear relationship between the eastward electric field enhancement near the sunset and the seasonal/longitudinal distribution of the spread F occurrence across the solar epoch (Fejer et al., 1999; Huang, 2018; Stolle et al., 2008; Whalen, 2002). The PRE of the zonal electric field around the local sunset uplifts the F layer into the altitudinal region suitable for the rapid plasma irregularity growth by the R–T instability mechanism. Thus, the vertical drift amplitude has been described as the dominant factor influencing the difference in the observed features, such as the onset time, the occurrence rate or the latitudinal extension of the plasma irregularity across the various seasons or longitudes.

However, other factors such as the zonal drift reversal could also significantly impact the post-sunset electrodynamic effect on the observed plasma irregularity features across different seasons; for example, the delayed (2 h lag) RSF onset time during the M -equinox and J -solstice of the LSA compared with the observed characteristics at KWJ during the corresponding seasons of the MSA period, shown in Figs. 4 and 5. This is attributed to the delayed zonal drift reversal effect on the instability growth rate during the LSA (Su et al., 2009). The eastward reversal of the zonal plasma drift in the upper ionosphere region causes a vertical shear motion and the initiation of the irregularity growth (Kudeki and Bhattacharyya, 1999). Su et al. (2009) presented a theoretical analysis of the zonal drift reversal effect on the post-sunset dynamics at the F region base using the simulation result obtained at the longitude of KWJ station during the J -solstice season. The zonal drift was expressed as follows:

$$V_{\Phi} = -\frac{\sigma_H}{\sigma_P} \frac{E_{\Phi}}{B} + U_{\Phi} + \frac{\sigma_H}{\sigma_P} U_p - \frac{J_p}{\sigma_P B}, \quad (2)$$

where σ_P and σ_H represent the Pedersen and Hall conductivities respectively; B is the magnetic field; E , U and J represent the electric field, neutral wind and current respectively;

and \mathbb{J} and Φ are the components in the vertical and zonal direction respectively. The average F region altitude near local sunset is above 200 km and $(\frac{\sigma_H}{\sigma_P})$ tends toward nil in this altitude range; hence, the first and third term in Eq. (1) are negligible. The zonal drift reversal delay was described as being strongly influenced and indirectly proportional to the flux tube integrated Pedersen conductivity. Hence, an expectedly denser ionosphere and a corresponding increase in the Pedersen conductivity during the MSA will cause an earlier zonal drift reversal and larger occurrence rate as shown in Fig. 5. Likewise, the significant difference between the irregularity onsets at both equinoxes could also be as a result of the seasonal variation of the zonal drift reversal. This assumption is due to the disappearance of the RSF onset time delay at KWJ during M -equinox of the MSA as shown in Fig. 5. However, further investigation might be required to ascertain that the same phenomenon was responsible for the delayed onset time during the M -equinox season of the LSA.

The observed asymmetry in the RSF occurrence percentage for equinoxes and solstices at the different longitudes during both solar epochs were shown to be controlled by entirely different mechanisms (Manju and Madhav Haridas, 2015; Tsunoda, 2010b). In the case of the equinox asymmetry, the occurrence percentage is higher during the S -equinox at the JIC, FZA and KWJ stations during the LSA period, whereas the CPN and the ILR stations show approximately equal occurrence percentage during both equinoctial seasons. The equinox asymmetry is most visible at the Brazilian and Peruvian longitude during the LSA. Figure 7a shows an approximately equal $h'F$ peak at both equinoxes, which is inconsistent with the observed RSF occurrence asymmetry across these longitudes during the LSA.

In contrast, the equinoctial asymmetry of the RSF occurrence during the MSA, as shown in Fig. 7b, conforms with the corresponding larger $h'F$ peak during the M -equinox season at these stations. Manju and Madhav Haridas (2015) explored the probable relationship between the observed equinox asymmetry in the threshold height ($h'F_c$), the ESF occurrence percentage and the O/N_2 ratio. This asymmetry was shown to have a strong solar flux dependence. They associated this with a significant difference between the expansions of the thermosphere at both equinoxes as the solar flux increases, which expectedly reflects on the defined $h'F_c$. This relationship between the thermospheric neutral compositions and the post-sunset dynamics of the F region have also been shown by the earlier studies (Batista et al., 1986; Qian et al., 2009).

The neutral density in the upper thermosphere is known to change with a variation in the O/N_2 ratio, and the post-sunset vertical drift was shown to have a directly proportional relationship with the neutral density (Batista et al., 1986; Manju and Madhav Haridas, 2015). Thus, the higher O/N_2 ratio during the M -equinox as reported by Manju and Madhav Haridas (2015) is expected to correspond to a higher

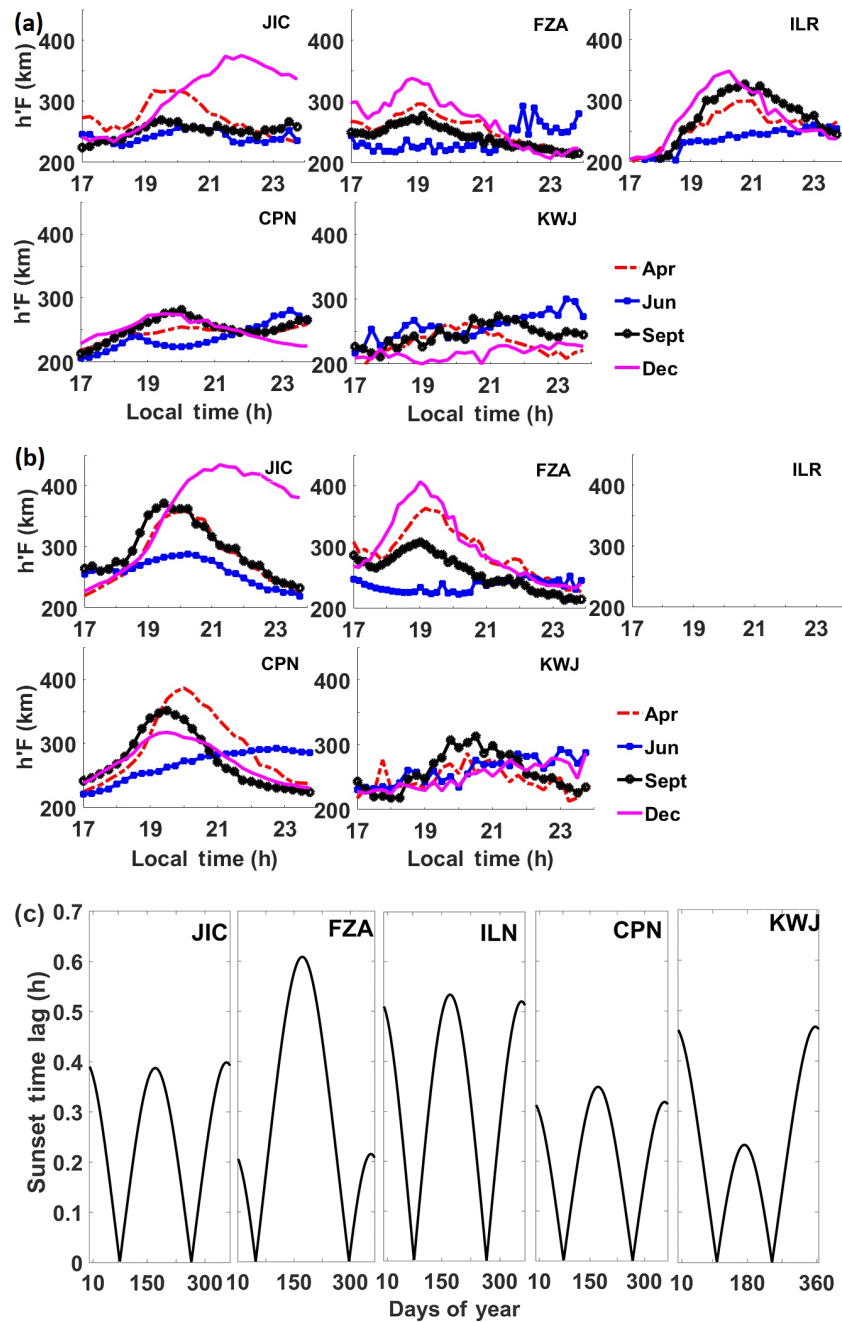


Figure 7. Monthly average of the virtual height during (a) MSA and (b) LSA. (c) The estimated sunset time lag between the geomagnetic conjugate points for each of the longitude sectors.

vertical drift peak during this period. Figure 7b presents a similar pattern in the estimated PSSR during the equinoctial months. The observed difference in the $h'F$ peak is more significant during the MSA, while during the LSA period, the observed PRE peak was approximately equal for both equinoxes across the different regions. According to Fig. 4, the Brazilian region recorded a large difference between the RSF occurrence percentages during the equinox seasons of the LSA period. The RSF occurrence percentage was larger

during the S-equinox season at the KWJ, JIC and FZA stations. This is attributed to the comparably reduced collision frequency effect on the irregularity growth rate due to the lower neutral density during this season. Consequently, the requisite PRE for the irregularity occurrence is smaller than the threshold during M-equinox (Manju and Madhav Haridas, 2015). Hence, the threshold height for RSF occurrence in a season would be dependent on the average neutral density during that season.

The decay of the EEJ current is relatively abrupt during the equinox in the large declination angle region, and the zonal drift reversal is directly related to the zonal wind reversal as described by Eq. (1). In the absence of the EEJ dependent factor, $(\frac{J_p}{\sigma_p B})$ in Eq. (1) will cause the zonal drift reversal to occur at almost the same time as the zonal wind and yields a strong background condition for the irregularity growth at both equinoxes. However, the sunset time lag tends to change rapidly in the large declination angle region, and Fig. 7c shows that it reaches almost twice the peak time lag at the small declination angle during the solstice season. As the sunset time lag increases, the short-circuiting effect on the post-sunset F region dynamo persists longer. This implies that the PSSR during the later days of the season will mostly fall below the defined threshold height for RSF occurrence during the *M*-equinox. An unpublished result taken at the FZA station showed that the RSF occurrence percentage reduces from March to April of the same LSA year by $\sim 40\%$. Conversely, the threshold height during the *S*-equinox is smaller, and the rapid change in the sunset time lag would have a lesser effect on the irregularity occurrence rate. Hence, the RSF occurrence percentage will be larger during the *S*-equinox in these longitude regions as described earlier. Coincidentally, the observed equinoctial asymmetry during the LSA seems to be more prevalent at stations with a larger declination angle. Madhav Haridas et al. (2015) analysed the role of the sunset time lag on the vertical drift peak in the Indian longitude region during the equinoxes and showed that the partial short-circuiting effect persists longer during the LSA and MSA periods. In the case of the small declination angle regions, we assume that the larger density during the *M*-equinox will cause a stronger suppression of the EEJ current effect and an earlier zonal drift reversal time. Thus, the seeding of the R–T instability occurs under a very conducive ionospheric condition for the optimal instability growth rate than during the *S*-equinox. The effect of the fourth term in Eq. (1) on the difference between the zonal drift at the two equinoxes might become more significant as the asymmetry in the neutral density increases during the MSA (Manju and Madhav Haridas, 2015).

The PSSR during the equinoxes shows a comparably similar pattern with the observed equinoctial asymmetry in the RSF occurrence percentage for all of the regions during MSA except in the Brazilian region (represented in Figs. 4 and 5). Where the RSF occurrence percentage peak was approximately equal for both equinox seasons. The American sector has the largest field-aligned Pedersen conductivity and we assume that the significant increase in the conductivity during MSA would nullify the asymmetry in the zonal drift reversal time in this region during equinoxes. On the contrary, this also means a significant increase in the ionospheric density and the threshold height. Hence, the inverse solar activity dependence of the RSF occurrence percentage observed at the JIC and FZA stations during the *S*-equinox, as shown

in Fig. 6a and b, is attributed to an increased density scale length. The observed large RSF occurrence percentage during the *S*-equinox of the LSA at these longitudes was earlier related to the effect of the contracted ionospheric density. However, the increase in the bottom-side density scale length during the MSA (Lee, 2010) will increase the threshold PRE for the irregularity occurrence (Smith et al., 2016). The inconsistent equinoctial asymmetry pattern at different solar flux indices was also observed in the Atlantic region during a study of the global equatorial plasma bubble occurrence (Gentile et al., 2006). A similar inverse solar activity pattern was observed in this longitude region by Su et al. (2007), as shown in their Fig. 3b, but it was less prominent than our result due to the difference in the altitude of the observations.

During the solstice seasons, the observed asymmetry in the PRE of the F layer and the RSF occurrence percentage at the low declination angle longitudes are inconsistent with the corresponding sunset time lag. Unlike the FZA and KWJ stations where the asymmetry between the solstices could be explained by the difference in the sunset time lag, the other three ionosonde stations have approximately the same sunset time lag at both solstices. The results showed a larger RSF occurrence percentage during the *D*-solstice at these longitudes. The significant asymmetry in the ionospheric density distribution during the solstice seasons is considered to be a probable factor in this case. There is post-sunset EEJ current due to large sunset time lag during the solstice seasons, which strongly affects the instability growth rate. The larger density during the *D*-solstice indicates an earlier zonal drift reversal and a more conducive ionospheric condition for the seeding of the R–T instability process (Su et al., 2009).

In a similar discussion, Tsunoda (2010a) attributed the observed asymmetry in the RSF occurrence during the solstices to the seasonal variation of the convective gravity wave (GW) sources at these longitudes and proposed the GW phase front and magnetic field line alignment (GWBA) hypothesis. This has been extensively discussed by previous studies (Li et al., 2016; Su et al., 2014; Tsunoda, 2010a), but further analysis is considered necessary to substantiate the correlation between the seasonal distribution of GW and RSF occurrence across these longitudes. However, the presence of a large GW amplitude is widely considered to be a requisite condition for the generation of spread F under a weak background ionospheric condition (Abdu et al., 2009; Manju et al., 2016). Therefore, the frequent GW occurrence recorded in the Asian and African regions (Su et al., 2014) and, consequently, the seeding effect are expected to have played a significant role in the observed plasma irregularity generation in this regions. Apart from the requisite GW and \vec{B} alignment, a large local electron density was described as an important prerequisite for the large ESF growth (Krall et al., 2013). The large electron density is considered necessary to support the GW-induced electric field and the plasma instability growth. Coincidentally, the peak electron density

in both regions (unpublished result) shows similar seasonal variation with the RSF occurrence percentage during LSA, as shown in Fig. 4. However, these plasma irregularities will be confined mostly to the low-altitude region, especially in the Asian region. This is due to the strong dependence of the altitudinal/latitudinal growth of irregularity on the PRE strength. The weak PRE at CPN results from the large magnetic field strength and small field-line-integrated conductivities in this longitude sector. Under such circumstance, the GW-induced perturbation electric field might be suppressed, and the impact on the instability growth across these longitudes may, therefore, be reduced in spite of the large GW frequency. An analysis based on satellite data would likely observe a significantly smaller RSF occurrence percentage in this region during this period. Likewise, Kil and Heelis (1998) reported that the longitudinal distribution of the ESF occurrence is dependent on the height of observation and that the occurrence probability at the low altitude could be related to the seed perturbation from the tropospheric source.

5 Conclusions

The statistical result of the hourly variation of the RSF occurrence percentage across different longitude sectors was investigated during the MSA and LSA period for stations close to the magnetic Equator. The manual observation of the seasonal variation of the RSF occurrence pattern using the ionogram data revealed the distinct RSF occurrence features in each of the regions. This highlighted the complex morphology of the ESF events and the diverse role of the different factors contributing to plasma irregularity initiation across the different longitudes during the MSA and LSA. The large RSF occurrence percentage in the West African region (ILR) under the weak ambient ionospheric condition of the LSA period was attributed to the presence of strong GW occurrence in the region. Other important observations included the varying longitudinal pattern of the equinoctial asymmetry during the LSA and MSA. The longitudinal/seasonal variation of the zonal drift reversal time effect on the RSF onset was associated with the observed inconsistency in the asymmetry pattern during the equinoctial seasons of both solar epochs. Likewise, an anti-solar activity variation of the ESF occurrence percentage was also observed at the JIC and FZA stations during the *S*-equinox. This was attributed to the possible role of an expected increase in the bottom-side density scale length with the solar flux index. The results presented show the significant effect of the zonal drift reversal time on the seeding of a plasma irregularity and, consequently, the number of irregularity occurrences during a season.

Data availability. The data used in this study can be accessed through the University of Massachusetts Lowell Global Ionospheric

Radio Observatory (GIRO) Digital Ionosonde Database and South-east Asia low-latitude ionospheric network (SEALION).

Author contributions. AAO: Conceived and designed analysis, Performed the analysis, Wrote the paper; SJM: Supervision and review; MA: Supervision and review; SMB: Supervision and review; TY: Contributed data; PS: Contributed data; TY: Contributed the ionosonde data (SEALION); PS: Contributed the ionosonde data (SEALION).

Competing interests. The authors declare that they have no conflict of interest.

Acknowledgements. The authors thank the institutions responsible for the ground-based observations and ionosonde database used in this study. Thanks are also due to Daniel Okoh and Oliver Montenbruck, who offered meaningful assistance with the estimation of the sunset time lag. Furthermore, the authors are grateful to the anonymous referees for their suggestions and evaluation of this paper.

Review statement. This paper was edited by Dalia Buresova and reviewed by three anonymous referees.

References

- Aarons, J., Mendillo, M., and Yantosca, R.: GPS phase fluctuations in the equatorial region during sunspot minimum, *Radio Sci.*, 32, 1535–1550, <https://doi.org/10.1029/97RS00664>, 1997.
- Abdu, M. A.: Outstanding problems in the equatorial ionosphere-thermosphere electrodynamics relevant to spread F, *J. Atmos. Sol.-Terr. Phys.*, 63, 869–884, [https://doi.org/10.1016/S1364-6826\(00\)00201-7](https://doi.org/10.1016/S1364-6826(00)00201-7), 2001.
- Abdu, M. A.: Electrodynamics of ionospheric weather over low latitudes, *Geosci. Lett.*, 3, 11, <https://doi.org/10.1186/s40562-016-0043-6>, 2016.
- Abdu, M. A., Bittencourt, J. A., and Batista, I. S.: Magnetic declination control of the equatorial F region dybamo electric field development and spread F, *J. Geophys. Res.*, 86, 1143–11446, <https://doi.org/10.1029/JA086iA13p11443>, 1981.
- Abdu, M. A., Batista, I. S., and Sobral, J. H. A.: A New Aspect of Magnetic Declination Control of Equatorial Spread F and F Region Dynamo, *J. Geophys. Res.-Space*, 97, 14897–14904, <https://doi.org/10.1029/92JA00826>, 1992.
- Abdu, M. A., Alam Kherani, E., Batista, I. S., de Paula, E. R., Fritts, D. C., and Sobral, J. H. A.: Gravity wave initiation of equatorial spread F/plasma bubble irregularities based on observational data from the SpreadFEx campaign, *Ann. Geophys.*, 27, 2607–2622, <https://doi.org/10.5194/angeo-27-2607-2009>, 2009.
- Aveiro, H. C., Denardini, C. M., and Abdu, M. A.: Climatology of gravity waves-induced electric fields in the equatorial E region, *J. Geophys. Res.-Space*, 114, A11308, <https://doi.org/10.1029/2009JA014177>, 2009.

- Balan, N., Liu, L., and Le, H.: A brief review of equatorial ionization anomaly and ionospheric irregularities, *Earth Planet. Phys.*, 2, 257–275, <https://doi.org/10.26464/epp2018025>, 2018.
- Basu, S., Basu, S., Aarons, J., McClure, J. P., and Cousins, M. D.: On the coexistence of kilometer- and meter-scale irregularities in the nighttime equatorial F region, *J. Geophys. Res.*, 83, 4219–4226, <https://doi.org/10.1029/JA083iA09p04219>, 1978.
- Batista, I. S., Abdu, M. A., and Bittencourt, J. A.: Equatorial F region vertical plasma drifts: Seasonal and longitudinal asymmetries in the American sector, *J. Geophys. Res.-Space*, 91, 12055–12064, <https://doi.org/10.1029/JA091iA11p12055>, 1986.
- Booker, H. G. and Wells, H. W.: Scattering of radio waves by the F-region of the ionosphere, *J. Geophys. Res.*, 43, 249–256, <https://doi.org/10.1029/TE043i003p0249>, 1938.
- Bowman, G. G.: A relationship between “spread-F” and the height of the F2 ionospheric layer, *Aust. J. Phys.*, 13, 69–72, <https://doi.org/10.1071/PH600069>, 1960.
- Bowman, G. G.: A review of some recent work on mid-latitude spread-F occurrence as detected by ionosondes, *J. Geomagn. Geoelectr.*, 42, 109–138, 1990.
- Bowman, G. G.: Short-term delays (hours) of ionospheric spread F occurrence at a range of latitudes, following geomagnetic activity, *J. Geophys. Res.-Atmos.*, 103, 627–634, <https://doi.org/10.1029/98JA00630>, 1998.
- Candido, C. M. N., Batista, I. S., Becker-Guedes, F., Abdu, M. A., Sobral, J. H. A., and Takahashi, H.: Spread F occurrence over a southern anomaly crest location in Brazil during June solstice of solar minimum activity, *J. Geophys. Res.*, 116, A06316, <https://doi.org/10.1029/2010JA016374>, 2011.
- Dabas, R. S., Singh, L., Lakshmi, D. R., Subramanyam, P., Chopra, P., and Garg, S. C.: Evolution and dynamics of equatorial plasma bubbles: Relationships to ExB drift, postsunset total electron content enhancements, and equatorial electrojet strength, *Radio Sci.*, 38, 1075, <https://doi.org/10.1029/2001RS002586>, 2003.
- Dao, T., Otsuka, Y., Shiokawa, K., Nishioka, M., Yamamoto, M., Buhari, S. M., Abdullah, M., and Husin, A.: Coordinated observations of postmidnight irregularities and thermospheric neutral winds and temperatures at low latitudes, *J. Geophys. Res.-Space*, 122, 504–518, <https://doi.org/10.1002/2017JA024048>, 2017.
- De Paula, E. R., Muella, M. T. A. H., Sobral, J. H. A., Abdu, M. A., Batista, I. S., Beach, T. L., and Groves, K. M.: Magnetic conjugate point observations of kilometer and hundred-meter scale irregularities and zonal drifts, *J. Geophys. Res.*, 115, A08307, <https://doi.org/10.1029/2010JA015383>, 2010.
- Eccles, J. V., St. Maurice, J. P., and Schunk, R. W.: Mechanisms underlying the prereversal enhancement of the vertical plasma drift in the low-latitude ionosphere, *J. Geophys. Res.-Space*, 120, 4950–4970, <https://doi.org/10.1002/2014JA020664>, 2015.
- Fejer, B. G., Scherliess, L., and de Paula, E. R.: Effects of the vertical plasma drift velocity on the generation and evolution of equatorial spread F, *J. Geophys. Res.-Space*, 104, 19859–19869, <https://doi.org/10.1029/1999JA900271>, 1999.
- Gentile, L. C., Burke, W. J., and Rich, F. J.: A global climatology for equatorial plasma bubbles in the topside ionosphere, *Ann. Geophys.*, 24, 163–172, <https://doi.org/10.5194/angeo-24-163-2006>, 2006.
- Haldoupis, C., Kelley, M. C., Hussey, G. C., and Shalimov, S.: Role of unstable sporadic-E layers in the generation of midlatitude spread F, *J. Geophys. Res.*, 108, 1446, <https://doi.org/10.1029/2003JA009956>, 2003.
- Heelis, R. A.: Electrodynamics in the low and middle latitude ionosphere: A tutorial, *J. Atmos. Sol.-Terr. Phys.*, 66, 825–838, <https://doi.org/10.1016/j.jastp.2004.01.034>, 2004.
- Hoang, T. L., Abdu, M. A., MacDougall, J., and Batista, I. S.: Longitudinal differences in the equatorial spread F characteristics between Vietnam and Brazil, *Adv. Space Res.*, 45, 351–360, <https://doi.org/10.1016/j.asr.2009.08.019>, 2010.
- Huang, C. S.: Effects of the postsunset vertical plasma drift on the generation of equatorial spread F, *Prog. Earth Planet. Sci.*, 5, 3, <https://doi.org/10.1186/s40645-017-0155-4>, 2018.
- Jiao, Y. and Morton, Y. T.: Comparison of the effect of high-latitude and equatorial ionospheric scintillation on GPS signals during the maximum of solar cycle 24, *Radio Sci.*, 50, 886–903, <https://doi.org/10.1002/2015RS005719>, 2015.
- Kil, H. and Heelis, R. A.: Global distribution of density irregularities in the equatorial ionosphere, *J. Geophys. Res.-Space*, 103, 407–417, <https://doi.org/10.1029/97ja02698>, 1998.
- Klingam, S., Supnithi, P., Rungraengwajiake, S., Tsugawa, T., Ishii, M., and Maruyama, T.: The occurrence of equatorial spread-F at conjugate stations in Southeast Asia, *Adv. Space Res.*, 55, 2139–2147, <https://doi.org/10.1016/j.asr.2014.10.003>, 2015.
- Krall, J., Huba, J. D., Joyce, G., and Hei, M.: Simulation of the seeding of equatorial spread F by circular gravity waves, *Geophys. Res. Lett.*, 40, 1–5, <https://doi.org/10.1029/2012GL054022>, 2013.
- Kudeki, E. and Bhattacharyya, S.: Postsunset vortex in equatorial F-region plasma drifts and implications for bottom-side spread-F, *J. Geophys. Res.-Space*, 104, 28163–28170, <https://doi.org/10.1029/1998JA900111>, 1999.
- Lee, C. C.: Occurrence and onset conditions of postsunset equatorial spread F at Jicamarca during solar minimum and maximum, *J. Geophys. Res.-Space*, 115, 1–7, <https://doi.org/10.1029/2010JA015650>, 2010.
- Lee, C. C., Liu, J. Y., Reinisch, B. W., Chen, W. S., and Chu, F. D.: The effects of the pre-reversal ExB drift, the EIA asymmetry, and magnetic activity on the equatorial spread F during solar maximum, *Ann. Geophys.*, 23, 745–751, <https://doi.org/10.5194/angeo-23-745-2005>, 2005.
- Li, G., Otsuka, Y., Ning, B., Abdu, M. A., Yamamoto, M., Wan, W., Liu, L., and Abadi, P.: Enhanced ionospheric plasma bubble generation in more active ITCZ, *Geophys. Res. Lett.*, 43, 2389–2395, <https://doi.org/10.1002/2016GL068145>, 2016.
- Madhav Haridas, M. K., Manju, G., and Pant, T. K.: On the solar activity variations of nocturnal F region vertical drifts covering two solar cycles in the Indian longitude sector, *J. Geophys. Res.-Space*, 120, 1445–1451, <https://doi.org/10.1002/2014JA020561>, 2015.
- Manju, G. and Madhav Haridas, M. K.: On the equinoctial asymmetry in the threshold height for the occurrence of equatorial spread F, *J. Atmos. Sol.-Terr. Phys.*, 124, 59–62, <https://doi.org/10.1016/j.jastp.2015.01.008>, 2015.
- Manju, G., Madhav Haridas, M. K., and Aswathy, R. P.: Role of gravity wave seed perturbations in ESF day-to-day variability: A quantitative approach, *Adv. Space Res.*, 57, 1021–1028, <https://doi.org/10.1016/j.asr.2015.12.019>, 2016.

- Maruyama, T. and Matuura, N.: Longitudinal variability of annual changes in activity of equatorial spread F and plasma bubbles, *J. Geophys. Res.*, 89, 10903, <https://doi.org/10.1029/JA089iA12p10903>, 1984.
- Maruyama, T., Saito, S., Kawamura, M., and Nozaki, K.: Thermospheric meridional winds as deduced from ionosonde chain at low and equatorial latitudes and their connection with midnight temperature maximum, *J. Geophys. Res.-Space*, 113, 1–9, <https://doi.org/10.1029/2008JA013031>, 2008.
- Miller, C. A.: Electrodynamics of midlatitude spread F 2. a new theory of gravity wave electric fields, *J. Geophys. Res.-Space*, 102, 11533–11538, <https://doi.org/10.1029/96JA03840>, 1997.
- Narayanan, V. L., Sau, S., Gurubaran, S., Shiokawa, K., Balan, N., Emperumal, K., and Sripathi, S.: A statistical study of satellite traces and evolution of equatorial spread F, *Earth Planet. Space*, 66, 160, <https://doi.org/10.1186/s40623-014-0160-4>, 2014.
- Otsuka, Y.: Review of the generation mechanisms of post-midnight irregularities in the equatorial and low-latitude ionosphere, *Prog. Earth Planet. Sci.*, 5, 57, <https://doi.org/10.1186/s40645-018-0212-7>, 2018.
- Pezzopane, M., Zuccheretti, E., Abadi, P., De Abreu, A. J., De Jesus, R., Fagundes, P. R., Supnithi, P., Rungraengwajake, S., Nagatsuma, T., Tsugawa, T., Cabrera, M. A., and Ezquer, R. G.: Low-latitude equinoctial spread-F occurrence at different longitude sectors under low solar activity, *Ann. Geophys.*, 31, 153–162, <https://doi.org/10.5194/angeo-31-153-2013>, 2013.
- Pietrella, M., Pezzopane, M., Fagundes, P. R., Jesus, R. De, Supnithi, P., Klingam, S., Ezquer, R. G., and Cabrera, M. A.: Journal of Atmospheric and Solar-Terrestrial Physics Equinoctial spread-F occurrence at low latitudes in different longitude sectors under moderate and high solar activity, *J. Atmos. Sol.-Terr. Phys.*, 164, e815–e818, <https://doi.org/10.1016/j.jastp.2017.07.007>, 2017.
- Qian, L., Solomon, S. C., and Kane, T. J.: Seasonal variation of thermospheric density and composition, *J. Geophys. Res.-Space*, 114, A01312, <https://doi.org/10.1029/2008JA013643>, 2009.
- Reinisch, B. W. and I. A. Galkin: Global ionospheric radio observatory (GIRO), *Earth Planet. Space*, 63, 377–381, 2011.
- Sastri, J. H., Ranganath Rao, H. N., Somayajulu, V. V., and Chandra, H.: Thermospheric meridional neutral winds associated with equatorial midnight temperature maximum (MTM), *Geophys. Res. Lett.*, 21, 825–828, <https://doi.org/10.1029/93GL03009>, 1994.
- Shi, J. K., Wang, G. J., Reinisch, B. W., Shang, S. P., Wang, X., Zhrebotsov, G., and Potekhin, A.: Relationship between strong range spread F and ionospheric scintillations observed in Hainan from 2003 to 2007, *J. Geophys. Res.-Space*, 116, 1–5, <https://doi.org/10.1029/2011JA016806>, 2011.
- Smith, J. M., Rodrigues, F. S., Fejer, B. G., and Milla, M. A.: Coherent and incoherent scatter radar study of the climatology and day-to-day variability of mean F region vertical drifts and equatorial spread F, *J. Geophys. Res.-Space*, 121, 1466–1482, <https://doi.org/10.1002/2015JA021934>, 2016.
- Stolle, C., Lür, H., and Fejer, B. G.: Relation between the occurrence rate of ESF and the equatorial vertical plasma drift velocity at sunset derived from global observations, *Ann. Geophys.*, 26, 3979–3988, <https://doi.org/10.5194/angeo-26-3979-2008>, 2008.
- Stoneback, R. A., Heelis, R. A., Burrell, A. G., Coley, W. R., Fejer, B. G., and Pacheco, E.: Observations of quiet time vertical ion drift in the equatorial ionosphere during the solar minimum period of 2009, *J. Geophys. Res.-Space*, 116, 327–338, <https://doi.org/10.1029/2011JA016712>, 2011.
- Su, S. Y., Chao, C. K., Liu, C. H., and Ho, H. H.: Meridional wind effect on anti-solar activity correlation of equatorial density irregularity distribution, *J. Geophys. Res.-Space*, 112, 1–11, <https://doi.org/10.1029/2007JA012261>, 2007.
- Su, S.-Y., Chao, C. K., and Liu, C. H.: On monthly/seasonal/longitudinal variations of equatorial irregularity occurrences and their relationship with the postsunset vertical drift velocities, *J. Geophys. Res.-Space*, 113, A05307, <https://doi.org/10.1029/2011JA016712>, 2008.
- Su, S. Y., Chao, C. K., and Liu, C. H.: Cause of different local time distribution in the postsunset equatorial ionospheric irregularity occurrences between June and December solstices, *J. Geophys. Res.-Space*, 114, A04321, <https://doi.org/10.1029/2008JA013858>, 2009.
- Su, S. Y., Wu, C. L., and Liu, C. H.: Correlation between the global occurrences of ionospheric irregularities and deep atmospheric convective clouds in the intertropical convergence zone (ITCZ), *Earth Planet. Space*, 66, 134, <https://doi.org/10.1186/1880-5981-66-134>, 2014.
- Tsunoda, R. T.: Control of the seasonal and longitudinal occurrence of equatorial scintillations by the longitudinal gradient in integrated Eregion Pedersen conductivity, *J. Geophys. Res.-Space*, 90, 447–456, <https://doi.org/10.1029/JA090iA01p00447>, 1985.
- Tsunoda, R. T.: On equatorial spread F: Establishing a seeding hypothesis, *J. Geophys. Res.-Space*, 115, A12303, <https://doi.org/10.1029/2010JA015564>, 2010a.
- Tsunoda, R. T.: On seeding equatorial spread F during solstices, *Geophys. Res. Lett.*, 37, L05102, <https://doi.org/10.1029/2010GL042576>, 2010b.
- Tsunoda, R. T., Nguyen, T. T., and Le, M. H.: Effects of tidal forcing, conductivity gradient, and active seeding on the climatology of equatorial spread F over Kwajalein, *J. Geophys. Res.-Space*, 120, 632–653, <https://doi.org/10.1002/2014JA020762>, 2015.
- Vichare, G. and Richmond, A. D.: Simulation study of the longitudinal variation of evening vertical ionospheric drifts at the magnetic equator during equinox, *J. Geophys. Res.-Space*, 110, 1–8, <https://doi.org/10.1029/2004JA010720>, 2005.
- Wang, G. J., Shi, J. K., Wang, Z., Wang, X., Romanova, E., Ratovsky, K., and Polekh, N. M.: Solar cycle variation of ionospheric parameters over the low latitude station Hainan, China, during 2002–2012 and its comparison with IRI-2012 model, *Adv. Space Res.*, 60, 381–395, <https://doi.org/10.1016/j.asr.2016.12.013>, 2017.
- Whalen, J. A.: Dependence of equatorial bubbles and bottomside spread F on season, magnetic activity, and E/B Drift velocity during solar maximum, *J. Geophys. Res.-Space*, 107, A2, <https://doi.org/10.1029/2001JA000039>, 2002.
- Woodman, R. F. and La Hoz, C.: Radar observations of F region equatorial irregularities, *J. Geophys. Res.*, 81, 5447–5466, <https://doi.org/10.1029/JA081i031p05447>, 1976.